

Incommensurate ground state of double-layer quantum Hall systems

C. B. Hanna,¹ A. H. MacDonald,² and S. M. Girvin³

¹Department of Physics, Boise State University, Boise, Idaho 83725

²Department of Physics, University of Texas, Dallas, Texas 78712

³Department of Physics, Indiana University, Bloomington, Indiana 47405

(Received 11 October 2000; published 7 March 2001)

Double-layer quantum Hall systems possess interlayer phase coherence at sufficiently small layer separations, even without interlayer tunneling. When interlayer tunneling is present, application of a sufficiently strong in-plane magnetic field $B_{\parallel} > B_c$ drives a commensurate-incommensurate (CI) transition to an incommensurate soliton-lattice (SL) state. We calculate the Hartree-Fock ground-state energy of the SL state for all values of B_{\parallel} within a gradient approximation, and use it to obtain the anisotropic SL stiffness, the Kosterlitz-Thouless melting temperature for the SL, and the SL magnetization. The in-plane differential magnetic susceptibility diverges as $|B_{\parallel} - B_c|^{-1}$ when the CI transition is approached from the SL state.

DOI: 10.1103/PhysRevB.63.125305

PACS number(s): 73.43.Cd, 64.70.Rh, 71.10.Pm, 71.45.Gm

I. INTRODUCTION

At sufficiently low particle densities and small layer separations, double-layer quantum Hall (2LQH) systems at total filling factor unity ($\nu_T = 1$) can be described as broken-symmetry states¹ that possess interlayer phase coherence, even in the absence of interlayer tunneling.² The 2LQH system can be mapped to an equivalent spin-1/2 system by equating ‘‘up’’ (‘‘down’’) pseudospins with electrons in the upper (lower) layer.^{3–5} (The electrons are assumed to have their real spins polarized.) The exchange energy between the electrons produces a pseudospin stiffness ρ_s that seeks to keep the pseudospins aligned locally. At a finite layer separation d , the direct (Hartree) energy produces a local capacitive charging energy that is minimized when the two layers have equal electron densities. Thus the expectation value of the z component of the pseudospin vanishes and the pseudospin system has an ‘‘easy-plane’’ anisotropy that gives the itinerant ferromagnet an XY symmetry^{4,5} (in the absence of interlayer tunneling). The expectation value of a pseudospin at location \mathbf{r} can therefore be specified by its angle $\theta(\mathbf{r})$ in the xy plane.

In the absence of interlayer tunneling, the 2LQH system picks out a particular global value of θ in the ground state, spontaneously breaking the $U(1)$ symmetry of the XY ferromagnet. This gives rise to a linearly dispersing Goldstone mode at long wavelengths.^{4,5} Recent measurements of the zero-bias tunneling conductance in 2LQH systems show a huge resonant enhancement when interlayer coherence is present.⁶ This enhancement is related to the Goldstone mode of the broken $U(1)$ symmetry, and it has been proposed that the dispersion of the Goldstone mode can be observed in tunneling conductance measurements by applying a weak parallel magnetic field.⁷ The XY pseudomagnet also possesses vortex excitations called ‘‘merons’’; unlike those in an ordinary ferromagnet, these vortices are electrically charged, and the lowest-energy charged excitations of the system consist of vorticity-neutral meron pairs.^{4,5} There is also a finite-temperature Kosterlitz-Thouless (KT) phase transition due to the XY symmetry and the finite pseudospin stiffness of the ferromagnet.

In the presence of interlayer tunneling, the $U(1)$ invariance associated with conservation of the charge difference between the two layers is lost. The finite interlayer tunneling t of the electrons acts as an effective Zeeman pseudofield of magnitude $2t$ along the pseudospin x axis and aligns the pseudospins, so that $\theta = 0$ in the ground state. The Goldstone mode disappears, and the collective mode becomes gapped. In the presence of interlayer tunneling, merons of opposite vorticity are bound together by a ‘‘string’’ that produces a linear attraction between the merons, eliminating the finite-temperature KT transition.^{4,8}

Murphy *et al.* investigated the effect of an in-plane magnetic field B_{\parallel} on 2LQH systems.⁹ By varying B_{\parallel} and studying the energy gap obtained from activation energy measurements of the longitudinal resistivity, they found evidence of a phase transition between two competing QH ground states at a critical value $B_{\parallel} = B_c$. These two ground states are understood in the pseudospin language as being due to a competition between the tunneling energy t and the exchange energy ρ_s .^{4,5} Read presented an appealing analysis of charged (meron pair) excitations in this system, focusing on the value of the charge gap near the commensurate-incommensurate transition.¹⁰

The presence of B_{\parallel} periodically shifts the phase of the tunneling matrix elements, resulting in an effective Zeeman field for the pseudospins that rotates along the planar direction perpendicular to \mathbf{B}_{\parallel} , with a wavelength $\phi_0/B_{\parallel}d$, which is the distance required to contain one flux quantum $\phi_0 = h/e$ between the layers. The net result is that for gradual variations of the pseudospin texture (gradual on the scale of the magnetic length $l \equiv \sqrt{\hbar/eB_{\perp}}$, where B_{\perp} is the strength of the magnetic field normal to the plane), the energy of the XY pseudospin system has the Pokrovsky-Talapov (PT) form^{11–13}

$$\mathcal{E} = \int d^2r \left[\frac{1}{2} \rho_s (\nabla \theta)^2 - \frac{t}{2\pi l^2} \cos(\theta + \mathbf{Q} \cdot \mathbf{r}) \right]. \quad (1.1)$$

up to a constant, where $\mathbf{Q} \equiv (2\pi d/\phi_0)\mathbf{B}_{\parallel} \times \hat{\mathbf{z}}$ defines the parallel magnetic-field wave vector,

$$t = t_0 e^{-Q^2 l^2 / 4} \sqrt{1 - m_z^2} \quad (1.2)$$

is the tunneling energy (where t_0 is the tunneling energy when $Q=0$),¹⁴ and

$$\rho_s = (1 - m_z^2) \rho_E \quad (1.3)$$

is the pseudospin stiffness within the Hartree-Fock Approximation (HFA). Here $m_z \equiv \nu_1 - \nu_2$ is the layer imbalance, and

$$\rho_E = \frac{e^2}{4\pi\epsilon l} \frac{1}{16\pi} \int_0^\infty dx x^2 e^{-x^2/2} e^{-xd/l} \quad (1.4)$$

is the interlayer exchange stiffness when the layers are balanced: $\nu_1 = \nu_2 = 1/2$ or $m_z = 0$. The layer separation is d , and ν_j is the filling factor of layer j .

For small Q (small B_{\parallel}), the ground-state energy is minimized by having the pseudospins point in the direction of the local (rotating) pseudospin Zeeman field, so that $\theta(\mathbf{r}) = -\mathbf{Q} \cdot \mathbf{r}$. This is the commensurate ground state, and it minimizes the pseudospin Zeeman (tunneling) energy. However, it does so at the expense of the exchange energy, since neighboring pseudospins are no longer parallel. In the limit of large Q , the cost in exchange energy for the pseudospins to align with the rapidly rotating Zeeman field is prohibitive, and the pseudospins become (nearly) uniformly polarized (constant θ), just as if $t \rightarrow 0$. The state with uniformly polarized pseudospin is the large- Q limit of the incommensurate state. It turns out that for all finite $B_{\parallel} > B_c$, the translational symmetry of the pseudospin polarization is broken, and a soliton-lattice (SL) state is obtained in the incommensurate phase.

The SL phase of the PT model can also undergo a separate finite-temperature dislocation-mediated KT transition that restores the translational symmetry.¹³ This work focuses on calculating the ground-state properties of the SL state, for all $B_{\parallel} > B_c$. Interestingly, it is not necessary to determine $\theta(\mathbf{r})$ in order to calculate the total energy of the system.^{12,13,15} From the total energy, we calculate thermodynamic quantities such as the SL stiffnesses, extending the results of Ref. 10 for the stiffnesses and the KT temperature to all B_{\parallel} . We also calculate the SL contribution to the magnetization and susceptibility, and discuss some possibilities of measuring these quantities experimentally.

The plan of this paper is as follows. In Sec. II, we discuss the single-soliton solutions that follow from the equation of motion obtained from the PT energy. For $Q > Q_c$ the solitons proliferate; in Sec. III, the interaction between soliton lines is discussed, and the separation between solitons as a function of Q/Q_c is derived. In Sec. IV, the compressional and shear elastic constants are analyzed, and an estimate is made of the Kosterlitz-Thouless temperature for melting the soliton lattice, as a function of Q . The interlayer phase coherent 2LQH state has a diamagnetic response to an applied in-plane magnetic field.¹⁶ Section V gives a calculation of the in-plane magnetization due to the 2LQH state, as a function of Q . We conclude with a summary of our results.

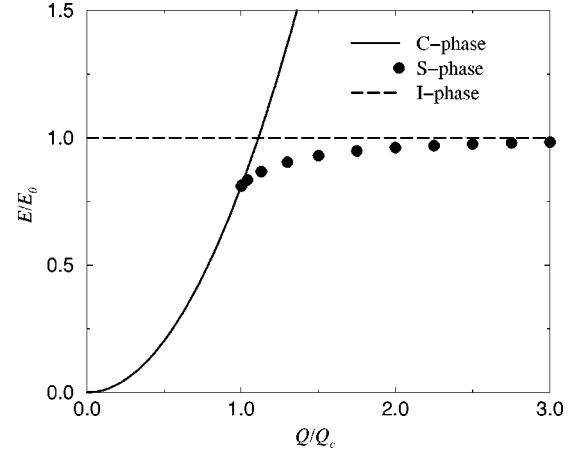


FIG. 1. Energy of the commensurate (C), the constant- θ incommensurate (I), and incommensurate SL (S) phases, vs the parallel magnetic-field wave vector Q . For $Q \geq Q_c$, the SL phase (dotted) has the lowest energy.

II. SINGLE SOLITONS

When $Q > Q_c$, it is convenient to define $\tilde{\theta}(\mathbf{r}) \equiv \theta(\mathbf{r}) + \mathbf{Q} \cdot \mathbf{r}$, so that Eq. (1.1) becomes

$$\mathcal{E} = \int d^2r \left[\frac{1}{2} \rho_s (\nabla \tilde{\theta} - \mathbf{Q})^2 - \frac{t}{2\pi l^2} \cos \tilde{\theta} \right]. \quad (2.1)$$

Minimizing \mathcal{E} with respect to variations in $\tilde{\theta}$ gives the sine-Gordon equation:

$$\nabla^2 \tilde{\theta} = \frac{1}{\xi^2} \sin \tilde{\theta}, \quad (2.2)$$

where $\xi/l = \sqrt{2\pi\rho_s}/t$. We shall give numerical values for our results for a hypothetical ‘‘typical’’ GaAs (effective mass $m^* \approx 0.07m_e$ and relative dielectric constant $\epsilon_r \approx 13$) 2LQH sample, which, for the sake of definiteness, we assign the following sample parameters: total particle areal density $n_T = 1.0 \times 10^{11} \text{ cm}^{-2}$, layer (midwell to midwell) separation $d = 20 \text{ nm}$, and tunneling energy $t_0 = 0.1 \text{ meV}$. Such a sample would have $l \approx 12.6 \text{ nm}$, $d/l \approx 1.6$, and $\hbar\omega_c \approx 6.9 \text{ meV}$ for $\nu_T = 1$, and $e^2/4\pi\epsilon l \approx 8.8 \text{ meV}$. In the HFA, $\rho_E \approx 0.03 \text{ meV}$ and $\xi \approx 17 \text{ nm}$.

The commensurate state minimizes the tunneling energy by having $\tilde{\theta}(\mathbf{r}) = 0$, so that the phase angle $\theta(\mathbf{r}) = \mathbf{Q} \cdot \mathbf{r}$ follows the tumbling Zeeman pseudofield. The energy per area of this state is $\rho_s Q^2/2 - t/2\pi l^2$. In the limit of large Q , the incommensurate state with constant θ has a lower energy per area, equal to zero. These energies are plotted as solid and dashed lines in Fig. 1. We therefore estimate that there is a phase transition near the point where the commensurate-state and the constant- θ incommensurate-state energies are equal, at $Q\xi \approx \sqrt{2}$. It turns out, however, that the incommensurate state lowers its energy by breaking translation invariance, so that, at finite t and $Q > Q_c$, the value of $\tilde{\theta}$ depends on position.

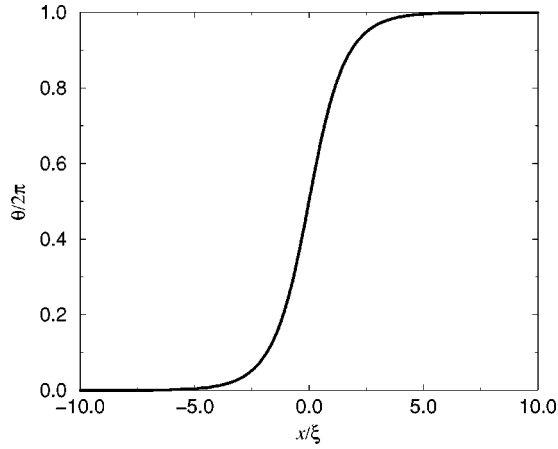


FIG. 2. At $Q = Q_c$, the system admits a single soliton, in which $\tilde{\theta}(\mathbf{r})$ twists by 2π over a distance ξ .

Equation (2.2) possesses soliton solutions. To see this, let us seek solutions of the form

$$\tilde{\theta}(\mathbf{r}) = \tilde{\theta}[\hat{\mathbf{e}}_1 \cdot (\mathbf{r} - \mathbf{r}_0)], \quad (2.3)$$

where $\hat{\mathbf{e}}_1$ could be any unit vector in the xy plane. Then Eq. (2.2) becomes

$$\partial_1^2 \tilde{\theta} = \frac{1}{\xi^2} \sin \tilde{\theta}. \quad (2.4)$$

Note that this equation is equivalent to the equation of motion for a pendulum of length l , $\partial_t^2 \phi = -(g/l) \sin \phi$, if we replace $\tilde{\theta} \rightarrow \phi - \pi$, $\hat{\mathbf{e}}_1 \cdot \mathbf{r} \rightarrow t$ (time), $\rho_s \rightarrow l$, and (tunneling amplitude) $t/2\pi l^2 \rightarrow g$. This analogy is very useful in finding the soliton solutions for the PT model. In particular, the pendulum can make full circles in a given direction. This corresponds to the SL state in the 2LQH system.

In analogy with the pendulum problem, we may define a conserved quantity analogous to the total (kinetic plus potential) energy of a pendulum:

$$2c^2 \equiv \frac{1}{2} \xi^2 (\partial_1 \tilde{\theta})^2 - (1 - \cos \tilde{\theta}). \quad (2.5)$$

Differentiating Eq. (2.5) with respect to $\hat{\mathbf{e}}_1 \cdot \mathbf{r}$, and using Eq. (2.4), shows that $\partial_1 c = 0$, so that c is a constant of the motion. Defining $\beta = \tilde{\theta}/2$ then leads to the equation

$$\partial_1 \beta = \pm \frac{1}{\xi} \sqrt{c^2 + \sin^2 \beta}. \quad (2.6)$$

It is straightforward to solve Eq. (2.6) when $c = 0$ by writing $f = \tan(\beta/2)$, so that $\partial_1 f = \pm f/\xi$, giving $\tilde{\theta} = \tilde{\theta}_{ss}(\mathbf{r})$, where

$$\tilde{\theta}_{ss}(\mathbf{r}) = 4 \arctan[e^{\pm \hat{\mathbf{e}}_1 \cdot (\mathbf{r} - \mathbf{r}_0)/\xi}] \quad (2.7)$$

represents a single soliton in the $\hat{\mathbf{e}}_1$ -direction, centered at $\hat{\mathbf{e}}_1 \cdot \mathbf{r}_0$, with width ξ . This is shown in Fig. 2. Note that $\tilde{\theta}_{ss}(\mathbf{r})$ changes by 2π as $\hat{\mathbf{e}}_1 \cdot \mathbf{r}$ goes from $-\infty$ to ∞ . This corre-

sponds to the motion of a pendulum that just barely completes a full revolution, and whose period goes to infinity.

The energy per length of a single soliton may be computed by substituting Eq. (2.7) into Eq. (2.1) and subtracting the commensurate-state ($\tilde{\theta} = 0$) energy, to obtain

$$\frac{\mathcal{E}_{ss}}{L_2} = \rho_s \left(\frac{8}{\xi} + 2\pi \hat{\mathbf{e}}_1 \cdot \mathbf{Q} \right), \quad (2.8)$$

where L_2 is the sample length in the planar direction perpendicular to $\hat{\mathbf{e}}_1$. The lowest (soliton) and highest (antisoliton) energy solutions occur for $\hat{\mathbf{e}}_1 = \pm \hat{\mathbf{Q}}$. Since solitons in the $-\hat{\mathbf{Q}}$ directions are equivalent to antisolitons in the $\hat{\mathbf{Q}}$ direction, we shall speak only about solitons with orientations defined by $\hat{\mathbf{e}}_1$. The lowest-energy soliton state has $\hat{\mathbf{e}}_1 = \hat{\mathbf{Q}}$, and its energy per length is

$$\frac{\bar{\mathcal{E}}_{ss}}{L_2} = 2\pi \rho_s (Q_c - Q), \quad (2.9)$$

which goes to zero when $Q = Q_c$, where

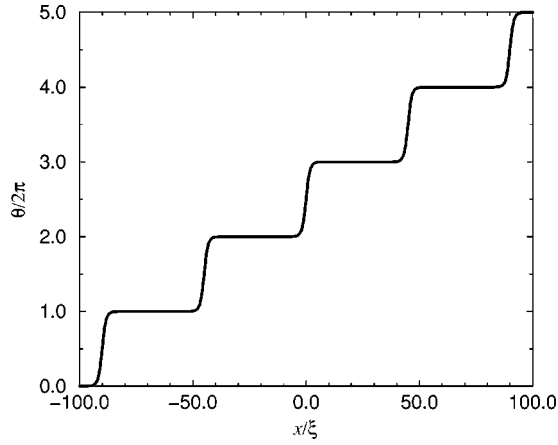
$$Q_c \equiv \frac{4}{\pi \xi} = \frac{4}{\pi} \sqrt{\frac{t/\rho_s}{2\pi l^2}}. \quad (2.10)$$

The value of the critical wave vector Q_c will depend on the layer imbalance $m_z \equiv \nu_1 - \nu_2$. Equations (1.2) and (1.3) give

$$Q_c(m_z) = (1 - m_z^2)^{-1/4} Q_c(0) \quad (2.11)$$

in the HFA, where $Q_c(0)$ is the value of Q_c when the layers are balanced ($m_z = 0$). Equation (2.11) implies that the value of Q_c where the CI transition occurs could be fine tuned by adjusting the layer imbalance m_z —i.e., by adjusting the gate voltages on the 2LQH sample. Such a procedure might be very useful in investigating the CI transition.

When $Q < Q_c$ and $t > 0$, the lowest-energy charged excitations are finite-length soliton lines with charged meron ends—i.e., charged vortices bound by a soliton “string” whose tension is given by Eq. (2.9). As Q increases, the soliton-line “string tension” becomes weaker, so that the Coulomb repulsion of the merons stretches out the string and lowers the energy of the charged excitation.² At $Q = Q_c$ the soliton-line “string tension” goes to zero, and it requires zero energy to make infinitely long soliton lines. Since the creation energy per length for a soliton decreases linearly with Q (with B_{\parallel}) for $Q \geq Q_c$, it becomes energetically favorable to form solitons. The number of solitons created is determined by the competition between the (negative) creation energy per soliton versus the repulsive (positive energy) interactions between solitons. Note that $Q_c < \sqrt{2}/\xi$ (the value of Q at which commensurate-state and constant- θ incommensurate-state energies are equal), so that for $Q > Q_c$ it is energetically favorable to create solitons. Because the solitons are weakly repulsive, the result is a soliton-lattice state that we describe below and illustrate in Fig. 3. An analogous effect occurs in long Josephson junctions, where application of a magnetic field parallel to two super-

FIG. 3. Soliton lattice for Q slightly larger than Q_c .

conducting planes in close proximity produces 2π twists in the Josephson phase and generates a SL state.^{17,18}

To summarize, for $Q < Q_c$, we obtain the commensurate phase in which $\tilde{\theta}(\mathbf{r}) = 0$. For $Q = Q_c$, we introduce a single soliton, corresponding to the marginal case of a pendulum

that makes exactly one full revolution and has an infinite period of oscillation. For $Q > Q_c$, we obtain a soliton lattice, corresponding to a pendulum making complete revolutions in one direction. It has been argued that the commensurate to incommensurate soliton-lattice (CI) transition at $Q = Q_c$ can be identified with the phase transition between 2LQH ground states seen by Murphy and co-workers;^{4,9} we therefore make the identification $Q_c = 2\pi B_c d / \phi_0$.

III. SOLITON LATTICE

We shall now use Eq. (2.6) to determine the SL spacing L_s . We do this by noting that over one period of the soliton lattice, $\tilde{\theta}$ changes by 2π , so that β changes by π . We therefore express L_s as

$$\frac{L_s}{\xi} = \frac{1}{\xi} \int_{-\pi/2}^{\pi/2} \frac{d\beta}{\partial_1 \beta} = 2 \int_0^{\pi/2} \frac{d\beta}{\sqrt{c^2 + \sin^2 \beta}} = 2\eta K(\eta), \quad (3.1)$$

where we have used Eq. (2.6) and have defined $\eta \equiv 1/\sqrt{c^2 + 1}$, and where

$$K(\eta) \equiv \int_0^{\pi/2} \frac{d\beta}{\sqrt{1 - \eta^2 \sin^2 \beta}} \rightarrow \begin{cases} \ln\left(\frac{4}{\sqrt{1 - \eta^2}}\right) + \frac{1}{4}(1 - \eta^2) \left[\ln\left(\frac{4}{\sqrt{1 - \eta^2}}\right) - 1 \right], & \eta \rightarrow 1 \\ \frac{\pi}{2} \left(1 + \frac{1}{4}\eta^2 + \frac{9}{64}\eta^4 \right), & \eta \rightarrow 0 \end{cases} \quad (3.2)$$

is the complete elliptic integral of the first kind.¹⁹ We define the SL wave vector $\mathbf{Q}_s \equiv (2\pi/L_s)\hat{\mathbf{e}}_1$, so that Eq. (3.1) may be written in terms of $Q_s \equiv |\mathbf{Q}_s|$ as

$$\frac{Q_s}{Q_c} = \frac{(\pi/2)^2}{\eta K(\eta)}. \quad (3.3)$$

Note that $\eta \rightarrow 1$ corresponds to the CI transition, where $Q_s \rightarrow 0$ and $Q \rightarrow Q_c$, whereas $\eta \rightarrow 0$ corresponds to the constant- θ incommensurate state, where $Q_s \rightarrow Q \rightarrow \infty$. From Eqs. (3.3) and (3.2), it follows that

$$\eta \rightarrow \begin{cases} 1 - 8e^{-2\pi/Q_s \xi}, & Q_s/Q_c \rightarrow 0 \\ \left(\frac{\pi Q_c}{2 Q_s} \right) \left[1 - \frac{1}{4} \left(\frac{\pi Q_c}{2 Q_s} \right)^2 + \frac{3}{64} \left(\frac{\pi Q_c}{2 Q_s} \right)^4 \right], & Q_s/Q_c \rightarrow \infty \end{cases} \quad (3.4)$$

In order to determine the value $\bar{\mathbf{Q}}_s$ of the SL wave vector that minimizes the total energy, we express the energy per area from Eq. (2.1) as an integral over β [cf. Eq. (3.1)], and obtain

$$\frac{\mathcal{E}}{L_1 L_2} = \frac{\rho_s}{\xi^2} \left[\left(\frac{1}{2} Q^2 - \mathbf{Q} \cdot \mathbf{Q}_s \right) \xi^2 + Q_c Q_s \xi^2 \frac{E(\eta)}{\eta} - \left(\frac{2}{\eta^2} - 1 \right) \right] \rightarrow \begin{cases} \frac{1}{2} \rho_s Q^2 - t/2\pi l^2, & Q < Q_c \\ \rho_s \left[\frac{1}{2} Q^2 - \mathbf{Q} \cdot \mathbf{Q}_s + Q_c Q_s (1 + 4e^{-2\pi/Q_s \xi}) - 1/\xi^2 \right], & \eta \rightarrow 1 \\ \rho_s \left[\frac{1}{2} (\mathbf{Q} - \mathbf{Q}_s)^2 - 1/(2Q_s \xi^2) \right], & \eta \rightarrow 0, \end{cases} \quad (3.5)$$

where

$$E(\eta) \equiv \int_0^{\pi/2} d\beta \sqrt{1 - \eta^2 \sin^2 \beta} \rightarrow \begin{cases} 1 + \frac{1}{2}(1 - \eta^2) \left[\ln \left(\frac{4}{\sqrt{1 - \eta^2}} \right) - \frac{1}{2} \right], & \eta \rightarrow 1 \\ \frac{\pi}{2} \left(1 - \frac{1}{4} \eta^2 - \frac{3}{64} \eta^4 \right), & \eta \rightarrow 0 \end{cases} \quad (3.6)$$

is the complete elliptic integral of the second kind,¹⁹ and L_1 is the sample length in the planar direction parallel to $\hat{\mathbf{e}}_1$. Agreement between Eqs. (2.8) and (3.5) in the thermodynamic limit is obtained by equating $\mathbf{Q}_s = (2\pi/L_1)\hat{\mathbf{e}}_1$, so that $L_s = L_1$ at $Q = Q_c$.

All the terms in the $\eta \rightarrow 1$ limit (near the CI transition, where the solitons are well separated) of Eq. (3.5) have simple physical interpretations. The first and last terms, $\rho_s(Q^2/2 - 1/\xi^2)$, constitute the (commensurate-phase) energy per area of the PT model in the absence of solitons. The second and third terms, $\rho_s(Q_c Q_s - \mathbf{Q} \cdot \mathbf{Q}_s)$ are just the creation energy per area for the solitons in terms of interacting soliton lines [see Eq. (2.9)]. The fourth term, $4\rho_s Q_c Q_s \exp(-2\pi/Q_s \xi)$, is the exponentially weak repulsive interaction energy per area between the solitons. Because $Q_s/2\pi = 1/L_s$ is the density of soliton lines, the fourth term shows that, near the CI transition, the interaction energy per length between two parallel, straight, and infinitely long soliton lines separated by a distance L_s is

$$\lim_{\eta \rightarrow 1} \frac{U}{L_y} \rightarrow 8\pi\rho_s Q_c e^{-L_s/\xi}. \quad (3.7)$$

Hence for $Q > Q_c$ soliton lines proliferate rapidly until the repulsion between the solitons become significant. The notion of an effective repulsive interaction between sine-Gordon solitons was discussed by Perring and Skyrme,¹⁵ who obtained the exponentially weak repulsion found above. The arguments of Ref. 15 implied that when the solitons are close together ($L_s/\xi \rightarrow 0$) at large Q/Q_c , the repulsive potential energy per length between soliton lines is $(\pi^3/2)\rho_s Q_c (\xi/L_s)$. This latter repulsion is due to boundary condition that $\bar{\theta}$ must change by 2π over the small distance

L_s , which implies a large gradient energy.

The value of \mathbf{Q}_s which minimizes the energy per area [Eq. (3.5)] is found by setting to zero

$$\frac{\partial}{\partial \mathbf{Q}_s} \left(\frac{\mathcal{E}}{L_1 L_2} \right) = \rho_s \left[Q_c \frac{E(\eta)}{\eta} \hat{\mathbf{Q}}_s - \mathbf{Q} \right], \quad (3.8)$$

where we have used the identity¹⁹

$$\frac{dE}{d\eta} = \frac{E(\eta) - K(\eta)}{\eta}. \quad (3.9)$$

It is not difficult to show that the second derivative of the energy per area with respect to Q_s is always positive; thus the extremum calculated above is a minimum. It follows from Eq. (3.8) that the energy is minimized for $\hat{\mathbf{Q}}_s = \hat{\mathbf{Q}}$ and for $\eta = \bar{\eta}$ such that

$$\frac{Q}{Q_c} = \frac{E(\bar{\eta})}{\bar{\eta}}, \quad (3.10)$$

where $Q \equiv |\mathbf{Q}|$.

We define the CI closeness parameter

$$\epsilon \equiv Q/Q_c - 1, \quad (3.11)$$

which vanishes at the CI transition; from Eqs. (3.6) and (3.10), it follows that, for $\bar{\eta} \rightarrow 1$,

$$\epsilon \approx \left(\frac{1 - \bar{\eta}}{2} \right) \left[\ln \left(\frac{8}{1 - \bar{\eta}} \right) + 1 \right], \quad (3.12)$$

so that, asymptotically,

$$\bar{\eta} \rightarrow \begin{cases} 1 - 2\epsilon/\ln(1/\epsilon), & Q_s/Q_c \rightarrow 0 \\ \left(\frac{\pi Q_c}{2 Q} \right) \left[1 - \frac{1}{4} \left(\frac{\pi Q_c}{2 Q} \right)^2 + \frac{5}{64} \left(\frac{\pi Q_c}{2 Q} \right)^4 \right], & Q_s/Q_c \rightarrow \infty \end{cases} \quad (3.13)$$

Equations (3.3) and (3.10) together allow us to determine the equilibrium SL wave vector $\bar{\mathbf{Q}}_s(\mathbf{Q})$ that minimizes the energy, in terms of the parallel-field wave vector \mathbf{Q} .²⁰ We have plotted this in Fig. 4. From Eqs. (3.3), (3.10), and (3.13), it follows that

$$\frac{\bar{Q}_s}{Q} = \frac{(\pi/2)^2}{K(\bar{\eta})E(\bar{\eta})} \rightarrow \begin{cases} (\pi^2/2)/\ln(1/\epsilon), & Q/Q_c \rightarrow 1 \\ 1 - \frac{1}{32} \left(\frac{\pi Q_c}{2 Q} \right)^4, & Q/Q_c \rightarrow \infty, \end{cases} \quad (3.14)$$

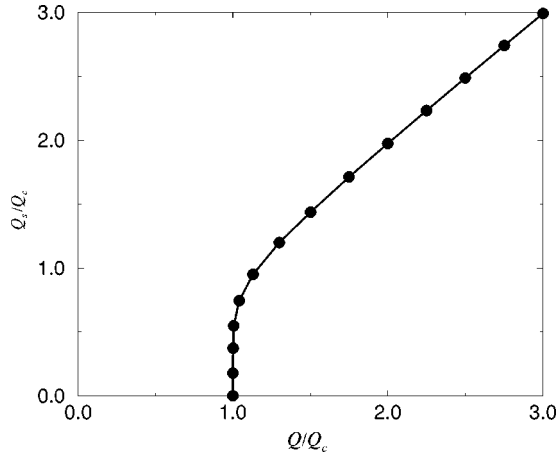


FIG. 4. Soliton wave vector \bar{Q}_s vs the in-plane magnetic-field wave vector Q . As $Q \rightarrow Q_c$, $\bar{Q}_s \xi \sim 2\pi/\ln[Q_c/(Q-Q_c)]$.

where the $Q \rightarrow Q_c$ limit is true asymptotically.^{10,12,21} We note, however, that, as found by Pokrovsky and Talapov¹¹ and discussed in Ref. 22, the meandering of soliton lines at finite temperature renormalizes the dependence of the soliton density on the parallel magnetic field, so that $Q_s \propto \sqrt{\epsilon}$ sufficiently close to the CI transition.

The minimized value \bar{E}/L_1L_2 of the energy per area at $Q_s = \bar{Q}_s$ is found by using Eqs. (3.5) and (3.10) in Eq. (3.6) to obtain

$$\begin{aligned} \frac{\bar{E}}{L_1L_2} &= \frac{1}{2}\rho_s Q^2 - \frac{t}{2\pi l^2} \left(\frac{2}{\eta^2} - 1 \right) \\ &\rightarrow \begin{cases} \frac{1}{2}\rho_s Q^2 - t/2\pi l^2, & Q < Q_c \\ -\frac{1}{2}\rho_s Q_c^2 (\pi^2/8 - 1), & Q/Q_c \rightarrow 1 \\ -\frac{t}{2\pi l^2} \frac{1}{16} \left(\frac{\pi Q_c}{2Q} \right)^2, & Q/Q_c \rightarrow \infty. \end{cases} \end{aligned} \quad (3.15)$$

The SL state energy per area is represented by the dots in Fig. 1.

Although it is not needed for calculating the stiffnesses or susceptibility of the SL, the SL solution for $\tilde{\theta}(\mathbf{r})$ is given by¹⁸

$$\sin\left[\frac{1}{2}(\tilde{\theta} - \pi)\right] = \text{sn}[\hat{\mathbf{e}}_1 \cdot (\mathbf{r} - \mathbf{r}_0)/\eta\xi, \eta], \quad (3.16)$$

where sn denotes the sine-amplitude Jacobian elliptic function with parameter η .¹⁹ Near the CI transition, when $Q \rightarrow Q_c$, $\tilde{\theta}$ is very close to being a periodic superposition of single-soliton solutions, spaced apart by $\bar{\mathbf{L}}_s$, so that $\tilde{\theta}(\mathbf{r}) \approx \sum_j \tilde{\theta}_{ss}(\mathbf{r} - j\bar{\mathbf{L}}_s)$, where $\tilde{\theta}_{ss}(\mathbf{r})$ denotes the single-soliton solution, Eq. (2.7). In the SL state, especially away from the CI transition, it is sometimes useful to work with

$$\theta_s(\mathbf{r}) \equiv \tilde{\theta}(\mathbf{r}) - \bar{Q}_s \cdot \mathbf{r} = \theta(\mathbf{r}) + (\mathbf{Q} - \bar{Q}_s) \cdot \mathbf{r}, \quad (3.17)$$

because it is periodic in the SL spacing, so that $\theta_s(\mathbf{r} + \bar{\mathbf{L}}_s) = \theta_s(\mathbf{r})$, where $\bar{\mathbf{L}}_s \equiv \bar{Q}_s 2\pi/\bar{Q}_s$. In the limit $Q/Q_c \rightarrow \infty$, $\bar{Q}_s \rightarrow \mathbf{Q}$ and $\theta_s \rightarrow \theta \rightarrow 0$, so that we may regard $\theta_s(\mathbf{r})$ as a small quantity. Expressing the sine-Gordon equation [Eq. (2.4)] in terms of θ_s and working to lowest order in θ_s gives $\nabla^2 \theta_s \approx (1/\xi^2) \sin[\bar{Q}_s \cdot (\mathbf{r} - \mathbf{r}_0)]$, so that

$$\lim_{Q \rightarrow \infty} \theta_s(\mathbf{r}) \approx - \left(\frac{\pi}{4} \frac{Q_c}{Q_s} \right)^2 \sin[\bar{Q}_s \cdot (\mathbf{r} - \mathbf{r}_0)]. \quad (3.18)$$

IV. STIFFNESSES OF THE SOLITON LATTICE

The elastic constants of the soliton lattice are given by the stiffness tensor K_{ij} . The change in the energy due to varying the spacing between the soliton lines is characterized by the compressional stiffness K_{11} . The shear stiffness K_{22} is associated with the change in energy due to shearing the upper and lower ends of the soliton lines in opposite directions, and is equivalent to a combined rotation and compression. We use the calculated stiffnesses to describe the B_{\parallel} dependence of the KT temperature¹⁰ for the dislocation-mediated KT melting transition¹³ of the soliton-lattice.

We calculate the stiffness tensor by two methods. First we calculate the stiffness K_{ij} that is obtained by differentiating \mathcal{E}/L_1L_2 in Eq. (3.5) with respect to the i and j components of Q_s for fixed Q at the extremal, where Eq. (3.8) is zero. Then we calculate the stiffness tensor \tilde{K}_{ij} obtained by calculating the effects of fluctuations of the angle variable $\tilde{\theta}(\mathbf{r})$ away from its ground-state value, Eq. (3.16).

We begin by calculating the stiffness tensor K_{ij} from the dependence of the ground-state energy [Eq. (3.5)] on the soliton-lattice wave vector Q_s . The expressions we obtain for K_{ij} by this method have been carried out for all values of $Q \geq Q_c$, and agree with the results obtained in Ref. 10, in the limit $Q \rightarrow Q_c$. Because the stiffnesses involve the second derivative of \mathcal{E}/L_1L_2 with respect to the components of Q_s at fixed Q , the terms in Eq. (3.5) that depend explicitly on Q (including the term $-\rho_s Q \cdot Q_s$ that gives the orientational dependence of the energy per area) do not contribute to K_{ij} . Thus

$$\begin{aligned} K_{ij} &= \lim_{Q_s \rightarrow \bar{Q}_s} \frac{\partial^2}{\partial Q_{si} \partial Q_{sj}} \left(\frac{\mathcal{E}}{L_1L_2} \right)_{\mathbf{Q}} \\ &= \rho_s Q_c \lim_{Q_s \rightarrow \bar{Q}_s} \frac{\partial}{\partial Q_{si}} \left[\frac{Q_{sj}}{Q_s} \frac{E(\eta)}{\eta} \right]_{\mathbf{Q}} \end{aligned} \quad (4.1)$$

$$\begin{aligned} &= \rho_s \lim_{Q_s \rightarrow \bar{Q}_s} \left[\left(\delta_{ij} - \frac{\bar{Q}_{si} \bar{Q}_{sj}}{\bar{Q}_s^2} \right) \frac{1}{\bar{Q}_s} + \frac{\bar{Q}_{si} \bar{Q}_{sj}}{\bar{Q}_s^2} \frac{\partial}{\partial Q_s} \right] \\ &\quad \times \left[Q_c \frac{E(\eta)}{\eta} \right]_{\mathbf{Q}}, \end{aligned} \quad (4.2)$$

where we have used Eqs. (3.8) and (3.10). Since $\bar{Q}_{s2} = 0$, it follows that $K_{12} = K_{21} = 0$.

Using the results of Sec. III, and the identity¹⁹

$$\frac{dK}{d\eta} = \frac{E(\eta)}{\eta(1-\eta^2)} - \frac{K(\eta)}{\eta}, \quad (4.3)$$

from which it follows that

$$\left(\frac{d\eta}{dQ_s}\right)_Q = -\frac{(\pi/2)^2(1-\eta^2)}{Q_c} \frac{E(\eta)}{E(\eta)} \left(\frac{Q_c}{Q_s}\right)^2, \quad (4.4)$$

we find that the compressional elastic constant K_{11} is equal to

$$\begin{aligned} \frac{K_{11}}{\rho_s} &= \lim_{Q_s \rightarrow \bar{Q}_s} \frac{\partial}{\partial \bar{Q}_s} \left[Q_c \frac{E(\eta)}{\eta} \right]_Q \\ &= \frac{\partial Q}{\partial \bar{Q}_s} \\ &= \frac{16(1-\bar{\eta}^2)}{(\bar{Q}_s \xi)^3 (Q \xi) \bar{\eta}^4} \rightarrow \begin{cases} (2/\pi^2) \epsilon \ln^2(1/\epsilon), & Q/Q_c \rightarrow 1 \\ 1 - \frac{3}{32} \left(\frac{\pi Q_c}{4 Q}\right)^4, & Q/Q_c \rightarrow \infty. \end{cases} \end{aligned} \quad (4.5)$$

In the limit $Q/Q_c \rightarrow 1$, when the soliton lines are far apart, K_{11} is very small [of order $\epsilon \sim \exp(-L_s/\xi)$; see Eq. (3.14)]. The energy cost of compression very close to the CI transition is due to the exponentially weak intersoliton interaction energy. The energy per area due to the string tension of the soliton lines (the term $\rho_s Q_c Q_s$) does not contribute to K_{11} , although it does contribute to K_{22} , as we explain below.

As explained in Ref. 23, soliton lines meander at finite temperature and are no longer straight; collisions between meandering soliton lines produce an effective entropic repulsion between the solitons, that dominates the exponential repulsion at any nonzero temperature, for L_s/ξ sufficiently large. This effect renormalizes the compressional stiffness K_{11} upwards so that it becomes proportional to T^2 . In the limit $Q/Q_c \rightarrow \infty$, the tunneling term in the PT energy [Eq. (2.1)] fluctuates on a very short length scale and averages to zero, so that Eq. (2.1) becomes the isotropic XY model; thus one expects K_{11} to approach the pseudospin stiffness ρ_s in that limit.

From Eqs. (3.10) and (4.1), it follows that the shear elastic constant K_{22} is given by

$$\frac{K_{22}}{\rho_s} = \frac{Q}{\bar{Q}_s} \rightarrow \begin{cases} (2/\pi^2) \ln(1/\epsilon), & Q/Q_c \rightarrow 1 \\ 1 + \frac{1}{2} \left(\frac{\pi Q_c}{4 Q}\right)^4, & Q/Q_c \rightarrow \infty. \end{cases} \quad (4.6)$$

As expected, the shear stiffness K_{22} approaches the pseudospin stiffness ρ_s in the limit $Q/Q_c \rightarrow \infty$. But in the limit $Q \rightarrow Q_c$, K_{22} diverges as Q_c/\bar{Q}_s . The origin of this effect is that the shear motion described by K_{22} increases the total length of the soliton lines. By definition, K_{22} describes a shear displacement in which Q_{s2} changes, while Q_{s1} remains

fixed: i.e., the soliton lines tilt away from their equilibrium ‘‘vertical’’ ($\hat{\mathbf{e}}_2$) direction by a small angle $\phi = Q_{s2}/Q_s$, while keeping their ‘‘horizontal separation’’ $\hat{\mathbf{e}}_1 \cdot \mathbf{L}_s = \bar{L}_s$ constant. This shear motion reduces the mean soliton separation (the separation along the direction perpendicular to the tilted soliton lines) to $L_s = \bar{L}_s \cos \phi$, so that $Q_s \rightarrow \bar{Q}_s / \cos \phi$. The K_{22} shear corresponds to a global rotation plus a compression of the SL. Packing the soliton lines more closely together in a fixed sample area produces more total soliton line length, which costs more soliton-line creation energy.

Because the term $-\rho_s \mathbf{Q} \cdot \mathbf{Q}_s$ that contains the orientational dependence of the energy per area [Eq. (3.5)] is linearly proportional to Q_{s1} , it cannot contribute to the stiffnesses (which are proportional to second derivatives of the energy per area with respect to the components of \mathbf{Q}_s) at all. It might be supposed that the rotation of the soliton lines that occurs upon shearing should cost energy, but this is not so, because a shear is a combination of rotation and compression, rather than a pure rotation. The creation energy per area of the SL near the CI transition ($Q \approx Q_c$) is $\rho_s (Q_c Q_s - \mathbf{Q} \cdot \mathbf{Q}_s)$, and consists of two terms. The first term ($\rho_s Q_c Q_s$) is just the total line length of the solitons times the line tension, divided by the total area. The second term ($-\rho_s \mathbf{Q} \cdot \mathbf{Q}_s$) depends explicitly on the angle ϕ between \mathbf{Q} and \mathbf{Q}_s , and determines the orientation of the SL because it is minimized by choosing \mathbf{Q}_s along Q (i.e., $\phi=0$); thus a different choice of SL orientation (i.e., a pure rotation of the soliton lines) would cost more energy. Interestingly, the second term in the creation energy is unchanged by a shear, because the energy cost of rotating the soliton lines is exactly offset by the increase in total soliton line length:

$-[Q(\bar{Q}_s/\cos \phi)] \cos \phi = -Q\bar{Q}_s$, independent of ϕ . The only change in the creation energy comes from the first term, which depends only on the density of soliton lines: $\rho_s Q_c (\bar{Q}_s/\cos \phi)$. Sufficiently close to the CI transition (i.e., when $L_s/\xi \gg 1$), the exponentially small interactions may be neglected in comparison to the creation energy. For $Q \rightarrow Q_c$ and small shear ($Q_{s2}/Q_{s1} \ll 1$),

$$\frac{\mathcal{E}}{L_1 L_2} \rightarrow \rho_s Q_c Q_s - t/2 \pi l^2 \approx \rho_s Q_c \left[Q_s + \frac{1}{2} \frac{Q_{s2}^2}{Q_s} \right] - t/2 \pi l^2, \quad (4.7)$$

so that $K_{22} \rightarrow \rho_s Q_c / \bar{Q}_s \rightarrow \infty$ as $Q \rightarrow Q_c$, in agreement with the results of Ref. 10.

The fact that bilayer phase-coherent 2LQH states can exhibit a finite-temperature KT transition in the absence of interlayer tunneling ($t \rightarrow 0$) was discussed in earlier work.^{4,5} Although finite t removes the possibility of a KT transition in the commensurate phase of 2LQH systems by altering the nature of the long-range interaction between vortices (‘‘merons’’ in this case),⁸ the SL phase does support a finite-

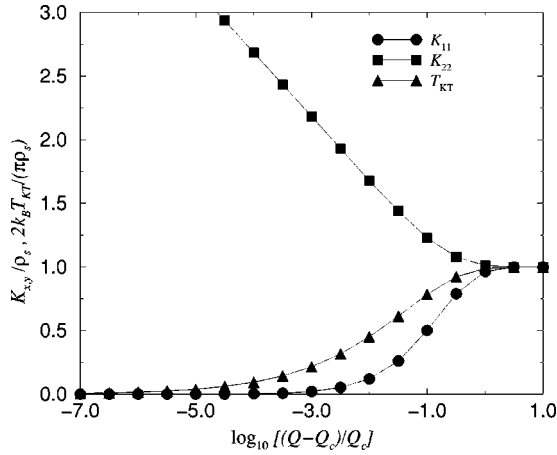


FIG. 5. Soliton-lattice stiffnesses $\rho_x \equiv K_{11}$ and $\rho_y \equiv K_{22}$, and their geometric mean, which is proportional to the Kosterlitz-Thouless temperature T_{KT} .

temperature KT transition due to dislocation-mediated melting of the SL.¹³ As discussed in Ref. 10, the KT temperature may be estimated as

$$\begin{aligned} \frac{k_B T_{KT}}{(\pi/2)\rho_s} &\sim \frac{1}{\rho_s} \sqrt{\det(K_{ij})} \\ &= \frac{1}{\rho_s} \sqrt{K_{11}K_{22}} \\ &\sim \frac{4\sqrt{1-\bar{\eta}^2}}{(\bar{Q}_s \xi)^2 \bar{\eta}^2} \rightarrow \begin{cases} (2/\pi^2) \sqrt{\epsilon \ln^3(1/\epsilon)}, & Q/Q_c \rightarrow 1 \\ 1 + \frac{13}{64} \left(\frac{\pi Q_c}{4 Q}\right)^4, & Q/Q_c \rightarrow \infty, \end{cases} \end{aligned} \quad (4.8)$$

where we have used the zero-temperature values for K_{ij} that we calculated previously to make a rough estimate of the KT temperature. As mentioned earlier, finite-temperature fluctuation effects can strongly renormalize K_{11} ,²³ and may also affect K_{22} . Our results agree with those of Ref. 10 in the limit $Q \rightarrow Q_c$. We have plotted the compressional (K_{11}) and shear (K_{22}) stiffnesses in Fig. 5, together with the KT temperature.

The KT transition would be most easily measured from the temperature dependence of the linear response to oppositely directed currents in each layer. This would require double-layer electron devices with layers that could be contacted separately. Unfortunately, the leakage currents produced when the interlayer tunneling is not vanishingly small would make it difficult, perhaps impossible, to set up oppositely directed currents in each layer. However, because the SL dislocations are electrically charged, it might be possible that the KT transition could be signaled by an increase in the usual longitudinal resistivity $\rho_{xx}(T)$, measured in devices with the current flowing in the same direction in both layers. The increase in $\rho_{xx}(T)$ would originate from the proliferation of unbound charged dislocations above the transition temperature.

We now calculate an alternate stiffness tensor \tilde{K}_{ij} by examining the effect of deviations of the angle variable $\tilde{\theta}(\mathbf{r})$ from its ground-state value. We write $\tilde{\theta}(\mathbf{r}) = \tilde{\theta}_0(\mathbf{r}) + \delta\tilde{\theta}(\mathbf{r})$, where $\tilde{\theta}_0(\mathbf{r})$ is the ground-state solution that minimizes the PT energy [Eq. (2.1)] and therefore satisfies Eq. (2.2), and $\delta\tilde{\theta}(\mathbf{r})$ is the deviation of $\tilde{\theta}$ from its ground-state value. We do not include dynamics here, because our focus is on ground-state, rather than excited-state, properties. The PT energy for $\tilde{\theta}$ is $E_{PT}[\tilde{\theta}_0 + \delta\tilde{\theta}] \equiv E_{PT}[\tilde{\theta}_0] + \delta H$, where E_{PT} , given by Eq. (2.1), is the PT energy from which the ground-state $\tilde{\theta}_0(\mathbf{r})$ is determined via Eq. (2.2), and

$$\begin{aligned} \delta H &\approx \frac{1}{2} \int \frac{d^2 r}{2\pi l^2} [t \cos \tilde{\theta}_0 \delta\tilde{\theta}^2 + 2\pi l^2 \rho_s (\nabla \delta\tilde{\theta})^2] \\ &= \frac{1}{2} \int \frac{d^2 r}{2\pi l^2} \delta\tilde{\theta} [t \cos \tilde{\theta}_0 - 2\pi l^2 \rho_s \nabla^2] \delta\tilde{\theta}, \end{aligned} \quad (4.9)$$

where we have kept terms up to quadratic order in $\delta\tilde{\theta}$. There are no terms linear in $\delta\tilde{\theta}$ because $\tilde{\theta}_0(\mathbf{r})$ is determined by minimizing E_{PT} with respect to variations in $\tilde{\theta}$. The total energy is minimized by choosing $\delta\tilde{\theta}$ from among the eigenvalues of the bracketed Schrödinger-like operator in Eq. (4.9), so that

$$[t \cos \tilde{\theta}_0 - 2\pi l^2 \rho_s \nabla^2] \delta\tilde{\theta}_q = \mathcal{E}_q \delta\tilde{\theta}_q. \quad (4.10)$$

If we take $\mathbf{B}_{\parallel} = B_{\parallel} \hat{\mathbf{y}}$, so that $\mathbf{Q} = Q \hat{\mathbf{x}}$, then $\tilde{\theta}_0(\mathbf{r})$ depends only on x , δH is translationally invariant in the y direction, and we may write $\delta\tilde{\theta}_q(\mathbf{r}) = \exp(iq_y y) \delta\tilde{\theta}_q(x)$. The term $t \cos \tilde{\theta}_0$ in Eq. (4.10) is periodic in the x direction, with a period of \bar{L}_s . As shown in Ref. 17, when $\tilde{\theta}_0(\mathbf{r})$ has the form of Eq. (3.16), Eq. (4.10) becomes Lamé's equation, after a simple rescaling of x . Lamé's equation has three simple solutions, two of which have low-energy limits. The first type of solution has zero energy and corresponds to a uniform translation of the vortex lines, $\delta\tilde{\theta} \propto \partial\tilde{\theta}_0/\partial x_0$, where x_0 is the x component of \mathbf{r}_0 in Eq. (3.16). Of greatest interest to us is the type of solutions which have been called ‘‘vortex oscillations’’ in the context of long Josephson junctions in parallel magnetic fields.¹⁸ From Ref. 18, it follows that in the long-wavelength limit,

$$\frac{\delta \mathcal{E}}{L_1 L_2} = \frac{1}{2} (K_{11} q_x^2 + \rho_s q_y^2), \quad (4.11)$$

where K_{11} is equal to the compressional stiffness in Eq. (4.5), and q_x is the crystal momentum along the x direction.

Although $\tilde{K}_{11} = K_{11}$, we find that $\tilde{K}_{22} = \rho_s \neq K_{22}$. The reason for the discrepancy between \tilde{K}_{22} and K_{22} is not obvious. It may be that using $K_{22} = Q/Q_s$ for the transverse stiffness is valid only at very long wavelengths $q_y < 1/Y_{SL}$,²⁴ where $Y_{SL} = L_s \sqrt{K_{22}/K_{11}}$ is Read's estimate of the minimum y distance for SL dislocations to interact logarithmically.¹⁰ It is also possible that \tilde{K}_{22} , which is based on a calculation that

assumes $\delta\tilde{\theta}$ is everywhere small, is not able to describe uniform shear, which can move soliton lines far from their equilibrium positions on the scale of the soliton line thickness ξ . The relationship between \tilde{K}_{22} and K_{22} requires further clarification, including a stronger argument for preferring K_{22} over \tilde{K}_{22} in estimating the KT temperature.

V. IN-PLANE MAGNETIZATION

The interlayer phase coherent 2LQH state exhibits an in-plane magnetization \mathbf{M}_{\parallel} in the presence of an in-plane magnetic field \mathbf{B}_{\parallel} . The in-plane magnetization can be calculated by differentiating the minimized ground-state energy per volume with respect to the parallel magnetic field,

$$\mathbf{M}_{\parallel} = -\frac{1}{L_1 L_2 d} \frac{\partial \bar{\mathcal{E}}}{\partial \mathbf{B}_{\parallel}} = -\frac{2\pi}{\phi_0} \hat{\mathbf{z}} \times \frac{\partial}{\partial \mathbf{Q}} \left(\frac{\bar{\mathcal{E}}}{L_1 L_2} \right), \quad (5.1)$$

where $\bar{\mathcal{E}}/L_1 L_2$ is given by Eq. (3.15). In order to carry out the differentiation in Eq. (5.1), we first differentiate Eq. (3.10) with respect to Q , and make use of Eq. (3.3), to obtain

$$\frac{\partial \bar{\eta}}{\partial Q} = -\left(\frac{2}{\pi}\right)^2 \bar{\eta}^3 \frac{\bar{Q}_s}{Q_c^2} (1 + Q^2 l^2/4). \quad (5.2)$$

We note here that the $Q^2 l^2/4$ term in Eq. (5.2) arises from differentiating Q_c in Eq. (3.10) with respect to Q ; the Q dependence of Q_c is due to the dependence of the tunneling matrix element on the parallel magnetic field, $t = t_0 \exp(-Q^2 l^2/4)$, which is a single-particle effect.¹⁴ The tunneling part of the equilibrium energy per area will also give a contribution to the in-plane magnetization proportional to $\partial t/\partial Q$, again due to dependence of t on Q . It is convenient to separate \mathbf{M}_{\parallel} into two parts: $\mathbf{M}_{\parallel} \equiv \mathbf{M}_{\text{SL}} + \mathbf{M}_t$, where \mathbf{M}_{SL} is calculated at fixed t (t independent of Q), and \mathbf{M}_t arises from the Q dependence of t .

Using Eqs. (5.1) and (5.2) it is straightforward to show that the SL contribution to the parallel magnetization is

$$\mathbf{M}_{\text{SL}} = -M_0 \hat{\mathbf{z}} \times (\mathbf{Q} - \bar{\mathbf{Q}}_s)/Q_c, \quad (5.3)$$

where

$$M_0 \equiv 2\pi\rho_s Q_c / \phi_0 \sim 0.5 \text{ A/m} \quad (5.4)$$

sets the scale of the SL magnetization, and the numerical estimate of M_0 is given for the ‘‘typical’’ GaAs sample described in Sec. II. For such a sample,

$$M_0 d = 2\pi\rho_s Q_c d / \phi_0 \sim 10^{-8} \text{ A} \quad (5.5)$$

sets the scale of the SL magnetic moment per unit area. Thus magnetometers with sensitivities in the range of 10^{-14} – 10^{-12} A m² would require sample areas in the range of 1 mm² and 1 cm² to measure M_{SL} . The magnitude of the SL magnetization behaves like

$$\left| \frac{M_{\text{SL}}}{M_0} \right| \rightarrow \begin{cases} 1 - (\pi^2/2)/\ln(1/\epsilon), & Q/Q_c \rightarrow 1 \\ \frac{\pi}{64} \left(\frac{\pi Q_c}{2Q} \right)^3, & Q/Q_c \rightarrow \infty. \end{cases} \quad (5.6)$$

The SL magnetization may also be calculated directly from the pseudospin supercurrent density,⁵ $\mathbf{J}_{zz} \equiv \mathbf{J}_1 - \mathbf{J}_2 = (2\rho_s/\hbar)\nabla\theta$, and the definition of the magnetic moment. The electrical current \mathbf{I} in layers 1 and 2 is

$$\mathbf{I} = \mathbf{I}_1 = -\mathbf{I}_2 = L_y (e\rho_s/\hbar)(\nabla\tilde{\theta} - \mathbf{Q}). \quad (5.7)$$

The magnetization produced by the above current is therefore²⁵

$$\begin{aligned} \mathbf{M}_{\text{SL}} &= \frac{1}{L_x L_y d} \hat{\mathbf{z}} \times \int \int \frac{\mathbf{I}}{c} dx dz = \frac{e\rho_s}{\hbar} \hat{\mathbf{z}} \times \frac{1}{L_x} \int_0^{L_x} (\nabla\tilde{\theta} - \mathbf{Q}) dx \\ &= -\frac{e\rho_s}{\hbar} \hat{\mathbf{z}} \times (\mathbf{Q} - \bar{\mathbf{Q}}_s), \end{aligned} \quad (5.8)$$

in agreement with Eq. (5.3).

The 2LQH interlayer phase-coherent state may be regarded as a pseudospin-channel superconductor.⁵ The magnetization \mathbf{M}_{\parallel} is due to pseudospin supercurrents, corresponding to electrical currents traveling in opposite directions in each layer, which partially screen \mathbf{B}_{\parallel} . For $Q < Q_c$, \mathbf{B}_{\parallel} is maximally excluded from the region between the planes; but when $Q \geq Q_c$, additional B_{\parallel} penetrates the region between the plates in the form of solitons that each carry a single flux quantum $\phi_0 = h/e$ (corresponding to a phase change $\Delta\tilde{\theta} = 2\pi$), leading to a precipitous decline in the magnetization. The direction of \mathbf{M}_{\parallel} is opposite to \mathbf{B}_{\parallel} , in accord with Lenz’s law. An exactly analogous effect occurs for magnetic fields applied parallel to narrow insulating regions (Josephson junctions) between superconductors.

The contribution to the magnetization due to the Q dependence of the tunneling matrix element t is

$$\mathbf{M}_t = -\frac{1}{2} \left(\frac{l}{\xi} \right)^2 M_0 \hat{\mathbf{z}} \times \left[\left(\frac{2}{\bar{\eta}^2} - 1 \right) \frac{\mathbf{Q}}{Q_c} - \frac{1}{2} \left(\frac{4Q}{\pi Q_c} \right)^2 \frac{\bar{\mathbf{Q}}_s}{Q_c} \right]. \quad (5.9)$$

In the commensurate phase, $\mathbf{M}_t = -(M_0/2)(l/\xi)^2 \hat{\mathbf{z}} \times \mathbf{Q}/Q_c$, and the magnitude of the tunneling contribution to the parallel magnetization behaves like

$$\left| \frac{M_t}{M_0} \right| \rightarrow \frac{1}{2} \left(\frac{l}{\xi} \right)^2 \begin{cases} 1 - 4/\ln(1/\epsilon), & Q/Q_c \rightarrow 1 \\ \frac{1}{2} (\pi/4)^2 (Q_c/Q), & Q/Q_c \rightarrow \infty. \end{cases} \quad (5.10)$$

The SL magnetization is plotted in Fig. 6. It is useful to compare the total SL magnetization M_0 to the scale of the Landau diamagnetism in a $\nu_T = 1$ 2LQH system,

$$\frac{M_0}{(n/d)\mu_B^*} = \frac{M_0 \phi_0 d}{\mu_B^* B_{\perp}} = 16 \frac{d}{\xi} \frac{\rho_s}{\hbar \omega_c} \sim 0.1, \quad (5.11)$$

where $\mu_B^* = e\hbar/2m^*$ is the effective Bohr magneton, and we have made use of the parameters for the ‘‘typical’’ GaAs sample described in Sec. II. This shows that the SL magnetization is expected to be roughly an order of magnitude smaller than the Landau diamagnetism. It is interesting to

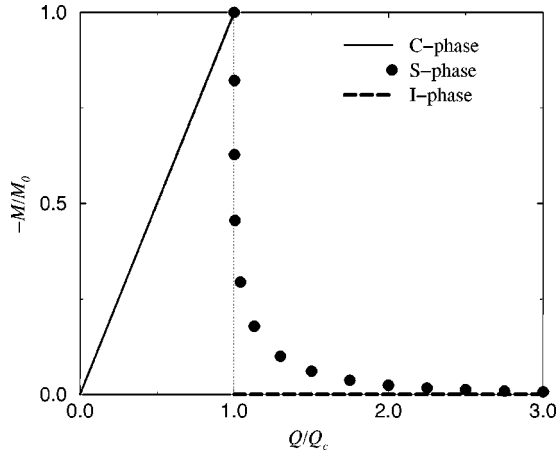


FIG. 6. SL contribution to the magnetization, which is proportional to $(Q - \bar{Q}_s)$, and therefore drops precipitously for $Q > Q_c$.

note that the weak signals associated with orbital diamagnetism in two-dimensional electron systems have been measured at high magnetic fields by torsional magnetometry,²⁶ superconducting quantum interference device magnetometry,²⁷ and micromechanical cantilever magnetometry.²⁸ The torque on the 2LQH sample in the presence of both a perpendicular and parallel magnetic field has both a Landau-diamagnetic component $\tau_{\perp} = (L_x L_y d) M_{\perp} B_{\parallel}$ and a SL component, $\tau_{\parallel} = (L_x L_y d) M_{\parallel} B_{\perp}$. The smallness of the parallel moment M_{\parallel} is offset by the large perpendicular magnetic field B_{\perp} in the expression for the torque τ_{\parallel} . The SL magnetization \mathbf{M}_{SL} might also be measured using high-field magnetometry techniques mentioned above.

It follows from Eq. (5.1) that when M_{\parallel} is plotted against B_{\parallel} , the area under the resulting curve from $B_{\parallel} = 0$ to $B_{\parallel} = \infty$ is

$$\int_0^{\infty} M_{\parallel} dB_{\parallel} = \frac{1}{L_x L_y d} [\bar{\mathcal{E}}(B_{\parallel} = \infty) - \bar{\mathcal{E}}(B_{\parallel} = 0)] = \left(\frac{t \langle m_x \rangle}{2\pi l^2 d} \right)_{B_{\parallel}=0}, \quad (5.12)$$

where $\langle m_x \rangle$ is the ground-state expectation value of the x component of the pseudospin order parameter, which has a value of $\sqrt{1 - m_z^2}$ in the HFA, so that $\langle m_x \rangle = 1$ (in the HFA) when the layers are balanced ($m_z = 0$). Thus the area under the M_{\parallel} versus B_{\parallel} curve may be regarded either as a measurement of t (if quantum fluctuations in the ground state are neglected), or as a measure of order-parameter suppression (of m_x) due to quantum fluctuations²⁹ (if t can be measured separately).

Equations (5.3) and (3.14) show that $\mathbf{M}_{\text{SL}} = -M_0 \hat{\mathbf{z}} \times \mathbf{Q}/Q_c = -(\chi_0/\mu_0) \mathbf{B}_{\parallel}$ in the commensurate phase ($Q < Q_c$), where $\chi_0 \equiv \mu_0 (2\pi/\phi_0)^2 \rho_s d$ sets the scale of the SL contribution to the magnetic susceptibility. The SL contribution to the parallel-field magnetic susceptibility is defined for fixed t (independent of Q):

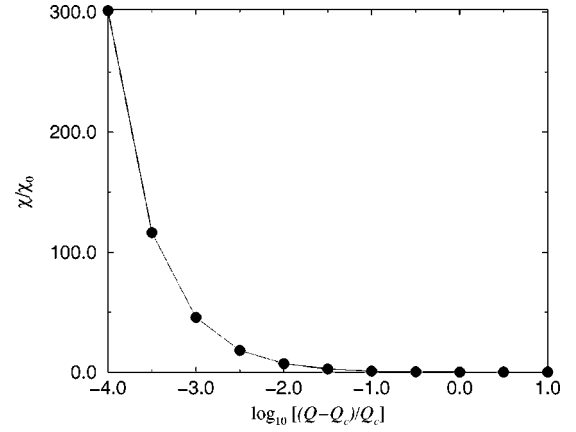


FIG. 7. SL contribution to the magnetic susceptibility, which diverges as $1/(Q - Q_c) \ln[Q_c/(Q - Q_c)]$ for $Q \rightarrow Q_c$.

$$\begin{aligned} \chi_{\text{SL}} &\equiv \mu_0 \left(\frac{\partial M_{\text{SL}}}{\partial B_{\parallel}} \right)_t \\ &= \mu_0 \frac{2\pi d}{\phi_0} \left(\frac{\partial M_{\text{SL}}}{\partial Q} \right)_t \\ &= \chi_0 \left(1 - \frac{\partial \bar{Q}_s}{\partial Q} \right)_t \\ &= \chi_0 \left(1 - \frac{\rho_s}{K_{11}} \right) \\ &\rightarrow \chi_0 \begin{cases} 1, & Q/Q_c < 1 \\ -(\pi^2/2)/[\epsilon \ln(1/\epsilon)], & Q/Q_c \rightarrow 1^+ \\ -\frac{3}{2} \left(\frac{\pi Q_c}{4 Q} \right)^4, & Q/Q_c \rightarrow \infty, \end{cases} \end{aligned} \quad (5.13)$$

where we have used Eqs. (3.10) and (4.5),

$$\chi_0 \equiv \mu_0 (2\pi/\phi_0)^2 \rho_s d = 4\pi\alpha^2 \epsilon_r \frac{d}{l} \left(\frac{\rho_s}{e^2/4\pi\epsilon l} \right) \sim 3 \times 10^{-7}, \quad (5.14)$$

and the numerical estimate of χ_0 is given for the ‘‘typical’’ GaAs sample described in Sec. II. Here $\alpha \approx 1/137$ is the fine-structure constant. We plot the susceptibility in Fig. 7. Note that near the CI transition, the susceptibility diverges like $1/(Q - Q_c)$, with logarithmic corrections.

It might be possible to measure the SL magnetization or even the SL magnetic susceptibility by varying the gate voltages of the sample, in order to adjust Q_c and tune close to the CI transition. Measuring χ_{SL} might be possible using ac modulation of the gate voltages in order to ac modulate the layer imbalance m_z and therefore the critical wave vector Q_c . By such a method, the ratio Q/Q_c could be ac modulated just above and below unity, allowing χ_{SL} to be determined at or near the CI transition. As an example, we compute here that part of $\partial M_{\text{SL}}/\partial m_z$ which is proportional to χ_{SL}

$$\begin{aligned}
\frac{\partial M_{\text{SL}}}{\partial m_z} &\sim \frac{\partial Q_c}{\partial m_z} \frac{\partial M_{\text{SL}}}{\partial Q_c} \\
&\sim -\frac{\partial Q_c}{\partial m_z} \frac{Q}{Q_c} \frac{\partial M_{\text{SL}}}{\partial Q} \\
&= -\frac{1}{\mu_0} \frac{\phi_0}{2\pi d} \frac{\partial Q_c}{\partial m_z} \frac{Q}{Q_c} \chi_{\text{SL}} = \frac{m_z}{1-m_z^2} \frac{M_0}{2} \frac{Q}{Q_c} \left(\frac{\rho_s}{K_{11}} - 1 \right),
\end{aligned} \tag{5.15}$$

where we have used Eq (2.11) in the last line. Equation (5.15) shows that $\partial M_{\text{SL}}/\partial m_z$ has a contribution proportional to χ_{SL} , which diverges like ρ_s/K_{11} near the CI transition. However, Eq. (5.15) vanishes for balanced layers ($m_z=0$); thus layer imbalance is required to measure $\partial M_{\text{SL}}/\partial m_z$. It turns out that when the layers are not balanced ($m_z \neq 0$), the solitons have a nonzero electric dipole moment per length;³⁰ this changes the intersoliton repulsion from being exponentially weak to being a power law. The net result is that the stiffness K_{11} near the CI transition is strengthened from being essentially linear in $(Q-Q_c)$ to being proportional to $\sqrt{Q-Q_c}$, so that the divergence in χ_{SL} becomes an inverse square-root singularity. In real samples, we expect this singularity to be smoothed out by finite temperature and disorder.

In practice, m_z is varied by adjusting gate voltages. For a small change δV_G in a gate voltage away from balance ($m_z=0$), the change δm_z in the layer imbalance is linearly proportional to δV_G . For the ‘‘typical’’ GaAs sample described in Sec. II, a rough estimate indicates that

$$\delta m_z \sim \frac{2\delta V_G}{eD_G n_T / (\epsilon_r \epsilon_0)} \sim 3\delta V_G/V, \tag{5.16}$$

if we take $D_G=10^{-6}$ m to be the distance between the gate and the double layers. There is an additional complication in changing the layer imbalance by adjusting one of the gate voltages. Unless both the back and front gates are adjusted together in a coordinated way, the change in gate voltage δV_G will also change the total filling factor ν_T by an amount $\delta \nu_T$, where

$$\delta \nu_T \sim \frac{\delta V_G}{eD_G n_T / (\epsilon_r \epsilon_0)} \sim 1.5\delta V_G/V, \tag{5.17}$$

if $D_G=10^{-6}$ m.

VI. SUMMARY

In the presence of a sufficiently strong parallel magnetic field, a $\nu_T=1$ 2LQH device undergoes a transition to a SL state. We have investigated the ground-state properties of the SL state for all values of the parallel magnetic field, with an eye toward possible experimentally measurable effects.

We found that the SL contribution to the orbital magnetization rises in the commensurate phase ($Q < Q_c$) with Q , and quickly drops to zero in the incommensurate phase ($Q > Q_c$). An estimate of the size of the SL magnetization shows that it could be detected by sensitive magnetometry techniques.^{26–28} The SL magnetic susceptibility shows a singularity at $Q=Q_c$, and it was proposed that this signature of the CI transition might be detected by varying the gate voltages so as to tune close to the CI transition.

The longitudinal and transverse SL stiffnesses were computed and used to estimate the temperature of the KT transition, which might be indicated experimentally by an increase in ρ_{xx} at the transition. A more sensitive signal of the KT transition would be obtained by measuring the transresistivity (Coulomb drag) as a function of temperature, although this would require separately contactable layers. However, the leakage currents produced by any sizable interlayer tunneling might make it impractical to set up oppositely directed currents in each layer.

In this paper, we have largely neglected the existence of disorder. As pointed out by Fisher³¹ and discussed by Read,¹⁰ randomness in the tunneling t , due, for example, to small variations in the barrier thickness, pins the SL domain walls randomly and destroys the long-range order, no matter how weak the randomness. This puts limits on how closely Q can approach Q_c — i.e., how small ϵ can be.

We have not discussed here the dynamics of the solitons — i.e., the motion of individual solitons³² or the collective motion of the SL (Ref. 33)—which also produce experimental signatures of the incommensurate SL state. We have focused instead on ground-state properties. One of us has recently found that when the layer densities are made unequal by adjusting the gate voltages of the device (keeping the total filling factor equal to one), the layer densities in the SL state become ‘‘rippled,’’ resulting in a dipole density wave.³⁰ Preliminary calculations show that the sudden onset of such a rippled SL state may give large contributions to the differential capacitance of 2LQH systems, especially for the interlayer capacitance (‘‘Eisenstein ratio’’).^{34,35} Further work on the properties of the rippled state is in progress, but it may be that sensitive measurements of differential capacitance in unbalanced ($\nu_1 \neq \nu_2$) 2LQH systems could detect the CI transition.

ACKNOWLEDGMENTS

C.B.H. would like to thank B. I. Halperin, N. Read, and T. C. Lubensky for helpful discussions, and the Institute for Theoretical Physics (ITP) at the University of California, Santa Barbara, where part of this work was carried out, for providing support through the ITP Scholars Program. This work was supported by an award from Research Corporation and by the National Science Foundation under Grant Nos. DMR-9972332, DMR-9714055, and DMR-0087133.

- ¹X. G. Wen and A. Zee, Phys. Rev. Lett. **69**, 1811 (1992); Phys. Rev. B **47**, 2265 (1993).
- ²For a review of double-layer quantum Hall systems, see the experimental chapter by J. P. Eisenstein and the theoretical chapter by S. M. Girvin and A. H. MacDonald, in *Novel Quantum Liquids in Low-Dimensional Semiconductor Structures*, edited by S. Das Sarma and A. Pinczuk (Wiley, New York, 1995).
- ³A. H. MacDonald, P. M. Platzmann, and G. S. Boebinger, Phys. Rev. Lett. **65**, 775 (1990).
- ⁴K. Yang, K. Moon, L. Zheng, A. H. MacDonald, S. M. Girvin, D. Yoshioka, and S. C. Zhang, Phys. Rev. Lett. **72**, 732 (1994).
- ⁵K. Moon, H. Mori, K. Yang, S. M. Girvin, A. H. MacDonald, L. Zheng, D. Yoshioka, and S. C. Zhang, Phys. Rev. B **51**, 5138 (1995).
- ⁶I. B. Spielman, J. P. Eisenstein, L. N. Pfeiffer, and K. W. West, Phys. Rev. Lett. **84**, 5808 (2000).
- ⁷Ady Stern, S. M. Girvin, A. H. MacDonald, and Ning Ma, cond-mat/0006457 (unpublished); Leon Balents and Leo Radzihovsky, cond-mat/0006450 (unpublished); Michael M. Fogler and Frank Wilczek (unpublished) cond-mat/0007403.
- ⁸K. Yang, K. Moon, L. Belkhir, H. Mori, S. M. Girvin, A. H. MacDonald, L. Zheng, and D. Yoshioka, Phys. Rev. B **54**, 11 644 (1996).
- ⁹S. Q. Murphy, J. P. Eisenstein, G. S. Boebinger, L. N. Pfeiffer, and K. W. West, Phys. Rev. Lett. **72**, 728 (1994).
- ¹⁰N. Read, Phys. Rev. B **52**, 1926 (1995).
- ¹¹V. L. Pokrovsky and A. L. Talapov, Phys. Rev. Lett. **42**, 65 (1970); Zh. Éksp. Teor. Fiz. **78** 269 (1980) [Sov. Phys. JETP **51**, 134 (1980)].
- ¹²P. Bak, Rep. Prog. Phys. **45**, 587 (1982).
- ¹³Marcel den Nijs, in *Phase Transitions in Critical Phenomena*, edited by C. Domb and J. L. Lebowitz (Academic Press, New York, 1988), Vol. 12, pp. 219–333.
- ¹⁴J. Hu and A. H. MacDonald, Phys. Rev. B **46**, 12 554 (1992).
- ¹⁵J. K. Perring and T. H. R. Skyrme, Nucl. Phys. **31**, 550 (1961).
- ¹⁶C. B. Hanna, A. H. MacDonald, and S. M. Girvin, Physica B **251**, 824 (1998).
- ¹⁷P. Lebwohl and M. J. Stephen, Phys. Rev. **163**, 376 (1967).
- ¹⁸A. L. Fetter and M. J. Stephen, Phys. Rev. **168**, 475 (1968).
- ¹⁹*Table of Integrals, Series, and Products*, edited by I. S. Gradshteyn and I. M. Ryzhik (Academic Press, New York, 1980), 4th ed., Sec. 8.1.
- ²⁰Equation (3.14) for \bar{Q}_s/Q and Eq. (3.10) for Q/Q_c in this work are equivalent to Eqs. (2.7) and (2.8), respectively, in Ref. 12, after correcting for misprints.
- ²¹F. C. Frank and J. H. Van der Merwe, Proc. R. Soc. London **198**, 205 (1949); **198** 216 (1949).
- ²²M. E. Fisher and D. S. Fisher, Phys. Rev. B **25**, 3192 (1982).
- ²³S. N. Coppersmith, D. S. Fisher, B. I. Haperin, P. A. Lee, and W. F. Brinkman, Phys. Rev. B **25**, 349 (1982).
- ²⁴N. Read (private communication).
- ²⁵*Classical Electrodynamics, 2nd ed.*, edited by J. D. Jackson (Wiley, New York, 1975), Sec. 5.6.
- ²⁶J. P. Eisenstein, H. L. Störmer, V. Narayanamurti, A. Y. Cho, A. C. Gossard, and C. W. Tu, Phys. Rev. Lett. **55**, 875 (1985); J. P. Eisenstein, H. L. Störmer, V. Narayanamurti, A. Y. Cho, and A. C. Gossard, Surf. Sci. **170**, 271 (1986); A. Potts, R. A. Shepherd, W. G. Herrenden-Harker, M. Elliot, C. L. Jones, A. Usher, G. A. C. Jones, D. A. Ritchie, E. H. Linfield, and M. Grimshaw, J. Phys.: Condens. Matter **8**, 5189 (1996); S. A. J. Wieggers, M. Specht, L. P. Levy, M. Y. Simmons, D. A. Ritchie, A. Cavanna, B. Etienne, G. Martinez, and P. Wyder, Physica B **251**, 115 (1998).
- ²⁷H. L. Störmer, T. Haavasoja, V. Narayanamurti, A. C. Gossard, and W. Wiegmann, J. Vac. Sci. Technol. B **1**, 423 (1983); Ines Meinel, Dirk Grundler, Silke Bargstädt-Franke, and Christian Heyn, Appl. Phys. Lett. **70**, 3305 (1997); I. Meinel, T. Hengstmann, D. Grundler, D. Heitmann, M. Bichler, and W. Wegscheider, Phys. Rev. Lett. **82**, 819 (1999).
- ²⁸M. P. Schwarz, D. Grundler, I. Meinel, Ch. Heyn, and D. Heitmann, Appl. Phys. Lett. **76**, 3564 (2000).
- ²⁹John Schliemann, S. M. Girvin, and A. H. MacDonald, cond-mat/0006309 (unpublished).
- ³⁰C. B. Hanna, Bull. Am. Phys. Soc. **43**, 496 (1998).
- ³¹M. P. A. Fisher (private communication).
- ³²Jordan Kyriakidis, Daniel Loss, and A. H. MacDonald, Phys. Rev. Lett. **83**, 1411 (1999); **85**, 2222(E) (2000).
- ³³R. Côté, L. Brey, H. Fertig, and A. H. MacDonald, Phys. Rev. B **51**, 13 475 (1995).
- ³⁴J. P. Eisenstein, L. N. Pfeiffer, and K. W. West, Phys. Rev. B **50**, 1760 (1994); Phys. Rev. Lett. **68**, 674 (1992).
- ³⁵T. Jungwirth and A. H. MacDonald, Phys. Rev. B **53**, 9943 (1996).